Desalination and Water Treatment
www.deswater.com

doi:10.5004/dwt.2018.22616

135 (2018) 341–350
December

A mesoporous biochar from bio-invasion alligator weed for adsorption of rhodamine B from aqueous solution

Yuan-da Du[a,1], Yu Feng[a,1], Li Shu[b], Zhao-jie Ren[c], Qiang Kong[a,*], Fei Xu[a], Qian Wang[a]

[a]*College of Geography and Environment, Shandong Normal University, 88 WenhuaDonglu, Jinan 250014, Shandong, China, email: 392331698@qq.com (Y.-d. Du), 1406490031@qq.com (Y. Feng), Tel. +86 531 86182550, Fax +86 531 86180107, email: kongqiang0531@hotmail.com (Q. Kong), xufeisdnu@yahoo.com (F. Xu), qianwang86@sdnu.edu.cn (Q. Wang)*
[b]*School of Engineering, RMIT University, 402 Swanston Street, Melbourne VIC 3000 Australia, e-mail: li.shu846@gmail.com (L. Shu)*
[c]*Nature department, Shandong Museum, No.11899 of Jingshi Road, Jinan 250014, China, email: 905793883@qq.com (Z.-j. Ren)*

Received 28 December 2017; Accepted 11 June 2018

ABSTRACT

Alligator weed, a malignant invasive weed worldwide, was used to prepare a low-cost and effective alligator weed biochar (AWBC) that adsorbs rhodamine B from aqueous solution. Scanning electron microscopy revealed that AWBC has a rough surface with a highly porous structure, a high surface area (736.3 m^2/g) and an abundant array of micropores and mesopores. The average pore size was 4.05 nm, which is predicted to improve the activated carbon adsorption performance of macromolecules and small molecule particles. Phosphorus-containing groups, C–H, C–O, and C=C moieties were present on the AWBC surface. Kinetic data obtained from three pollutants that were adsorbed by AWBC fit with a pseudo-second-order kinetic model ($R^2 > 0.99$), and this was considered as the rate-limiting factor for adsorption. The batch equilibrium data fitted well to the Langmuir isotherm ($R^2 > 0.99$), revealing monolayer adsorption and an adsorption capacity of 286 mg/g ($R^2 > 0.99$). Negative ΔG values confirmed the spontaneity of the adsorption process, and positive ΔH and ΔS values indicated endothermic and irreversible adsorption.

Keywords: Alligator weed; Biochar; Rhodamine B; Adsorption

1. Introduction

With the increasing use of chemical synthetic textiles in recent years, dyestuff wastewater has become one of the biggest contributors to pollution [1]. Dyestuff wastewater is mainly derived from the textile industry, and is characterized by high COD and BOD, high concentrations of reactive dyes, and the presence of refractory organic compounds [2,3]. Rhodamine B (RhB) is one of the most commonly used synthetic dyes, and has stable performance and good dyeing capacity. It is widely used in industrial production; including papermaking, textiles and cosmetics. RhB was formerly used as a food additive, but studies showing that it has teratogenic, carcinogenic and mutagenic effects on organisms have led to it being banned in foods [4]. Discharge of dyes into waterways not only is a great waste of resources, but also causes substantial harm to river and lake environments. Microbial metabolism degrades large amounts of organic matter in water, but this can also cause eutrophication. Additionally, enrichment of dyes in the food chain can lead to downstream teratogenic, carcinogenic and mutagenic effects [5,6].

Because RhB stability to photo-degradation, oxidising agents and bio-degradation. Therefore, removal of RhB is one of the main obstacles to dyestuff wastewater treatment, and traditional biological treatment methods do not completely removed the target dye pollutants in the wastewater [7]. Incomplete dye removal from wastewater can lead

*Corresponding author.

[1]These authors contributed equally to this work.

Presented at the 10th International Conference on Challenges in Environmental Science & Engineering (CESE-2017), 11–15 November 2017, Kunming, China

to toxic effects on aquatic organisms. Therefore, development of an efficient dye wastewater adsorption technology is the main goal of industrial and agricultural wastewater treatment research at this stage. To date, researchers have investigated various types of dye wastewater treatment; including the flocculation sedimentation (gas float) method [8], electrochemical oxidation [9] chemical oxidation [10], photocatalytic oxidation [11], the adsorption method [12] and biological oxidation [10]. The traditional physicochemical method is costly, difficult to operate and produces secondary pollution. Although the cost of the physicochemical method is relatively low in comparison with other methods, the structures of the intermediates produced are complex and the overall treatment effect is insignificant [13].

Activated carbon is an excellent adsorption material that has many advantages, including minimal equipment requirements, suitability in a wide range of pHs, and short operation periods. It has been widely applied in modern sewage treatment. Other adsorbent materials that are used include silica gel, ion exchange fiber, activated carbon, activated alumina, zeolite and fly ash [14–16]; however, these are very expensive. Therefore, in this study, we aimed to develop a low-cost adsorbent biochar from alligator weed that was suitable for removing RhB.

Alligator weed is a malignant invasive weed worldwide [17], and is widely distributed, cheap, and contains large quantities of lignin and cellulose. With its developed pore structure, it has potential for wastewater treatment following carbonizing with activated charcoal [18]. Adsorption of pollutants in the aqueous solution can also protect the environment. The study of alligator weed biochar (AWBC) has important theoretical and practical implications for understanding the adsorption properties of dye in wastewater, and developing a low-cost adsorbent material. The main objectives of this study were to investigate the preparation of biochar from alligator weed, and to characterize the physicochemical properties of AWBC. We also evaluated the kinetics, isotherms, and thermodynamics for RhB adsorption on AWBC.

2. Materials and methods

2.1. Biochar preparation

Alligator weed was obtained from Xiaoqing River, Jinan, Shandong Province. The weed was washed with distilled water and oven dried at 80°C for 24 h. Next, the alligator weed was cut it into 2–3 cm pieces using a high-speed grinder (HCP-100, Jinsui Company, Zhejiang). The small weed pieces were then soaked in 2% NaOH solution for 24 h. Next, the weed was washed with distilled water until the pH reached 6–7, and oven died at 120°C for 24 h. After drying, the weed was soaked in 85% phosphoric acid solution at RT for 6 h at a solid:liquid ratio of 1:4 (w/v). The weed mixture was then carbonized in a muffle furnace under the oxygen-deficient environment (Yong Guangming Company, Beijing) at 600°C for 1 h. (Yong Guangming Company, Beijing) at 600°C for 1 h. The biochar (BC) samples were then cooled to RT, washed with distilled water until the pH reached 6–7, and oven dried at 80°C for 2 d. Finally, the BC samples were cooled and ground into a powder that was could be passed through a 200-μm filter.

2.2. BC characterization

The adsorption properties of the BC were mainly determined by the large internal surface area. The specific surface structural morphology of the BC was characterized by scanning electron microscopy (SEM; SUPRATM55, Zeiss Company, Germany). The surface area analysis of the BC was performed using N_2 desorption-desorption isotherms (Quantachrome, USA). Brunauer-Emmett-Teller (BET) analysis was used to visualize the surface area and porosity and characterize the porous properties of the BC samples (Quantachrome, USA). A porosity analyzer (Quadrasorb SI, Quantachrome) was used to measure the pore size distribution and porosity of the BC. Fourier-transform infrared (FTIR) spectroscopy (Thermo Scientific, USA) was used to characterize the chemical functional groups on the BC surface in the 400–4000 cm^{-1} wavelength range.

2.3. Batch adsorption experiments

The RhB adsorption capacity of AWBC in aqueous solution was measured using three parallel batch adsorption experimental runs and one blank run. Five variables were investigated: the amount of AWBC, the initial RhB concentration, contact time, temperature, and pH. During the batch adsorption experiments, a 1000 mg/L RhB stock solution was diluted to the specified concentration and 50-mL aliquots were introduced into 100-mL conical flasks to give the desired dosage. To achieve an equilibrium state, the conical flasks were sealed and shaken in a temperature-controlled oscillator (HZQ-2, Jintan, Beijing) at a constant agitation speed of 180 rpm and a constant temperature. Afterwards, the samples were filtered through 0.22-μm microporous membranes to separate the AWBC from the RhB aqueous solution, and then the absorbances of the residual RhB filtrates were measured at 522 nm using an ultraviolet-visible spectrophotometer (T6-Xinshiji, Beijing).

The equilibrium adsorption capacity [Q_e (mg/g)] and removal rate [R(%)] of the AWBC in the equilibrium state are calculated as follows:

$$Q_e = \frac{(C_0 - C_e)V}{W} \tag{1}$$

$$R = \frac{(C_0 - C_e)}{C_0} \times 100 \tag{2}$$

where C_0 and C_e are the initial and equilibrium RhB concentrations, respectively (mg/L); V is the solution volume (L); and W is the BC mass (g).

2.4. Adsorption kinetics

The adsorption kinetics data were fitted to the pseudo-first and pseudo-second order kinetic models and the particle diffusion equation [19]. In the kinetics study, there were three parallel runs and one blank for the experiments. Twenty mg of AWBC was introduced into 50 mL RhB solutions at initial concentrations of 100, 150 and 250 mg/L at different time points (10, 30, 60, 90, 120, 150, 180, 240, 300, and 360 min).

The pseudo-first-order kinetic model is expressed as:

$$\ln\left(Q_e - Q_t\right) = Q_e K_1 t \tag{3}$$

where Q_e and Q_t are the amounts of RhB adsorbed (mg/g) at equilibrium and at time t (min), respectively; and k_1 (1/min) is the rate constant. Q_e and k_1 were obtained from a plot of ln ($Q_e - Q_t$) against t.

The pseudo-second-order equation is expressed as:

$$\frac{t}{Q_t} = \frac{1}{K_2 Q_e^{\,2}} + \frac{t}{Q_e} = \frac{1}{V_0} + \frac{t}{Q_e} \tag{4}$$

where k_2 (g/(mg min)) is the rate constant; Q_e and Q_t are the amounts of RhB adsorbed (mg/g) at equilibrium and at time t (min), respectively; and V_0 (mg g^{-1} min^{-1}) is the initial sorption rate. Q_e and k_2 were obtained from a plot of t/Q_t against t.

The particle diffusion equation is expressed as:

$$Q_t = k_p t^{\frac{1}{2}} + C \tag{5}$$

where k_p [mg/(g $min^{1/2}$)] is the rate constant. Both k_p and C were calculated from the fitted line of Q_t against $t^{1/2}$, and the boundary layer thickness was determined by C. If the plot of Q_t against $t^{1/2}$ is a straight line passing through the origin, the sole factor controlling the adsorption ratio is deemed to be intraparticle diffusion.

2.5. Adsorption isotherms

The correlation of the Langmuir, Freundlich, and Dubinin-Radushkevich model with the experimental data can help to determine the adsorption mechanism and the heterogeneity of the adsorbent material [20]. The AWBC performance was determined using an isotherm adsorption experiment to clarify the interaction between the AWBC and RhB. Three parallel runs and one blank were used for the experiments. Twenty mg of AWBC was introduced into 50 mL of RhB solution with six different initial concentrations (75, 100, 125, 150, 175, 200 mg/L RhB). Each adsorption isotherm experiment was placed in a temperature-controlled oscillator at 288 K, 298 K and 308 K. The correlation of the Langmuir, Freundlich, and Dubinin-Radushkevich model with the experimental data was used to examine the adsorption mechanism and the heterogeneity of the adsorbent.

The Langmuir model is expressed as:

$$\frac{C_e}{Q_e} = \frac{1}{Q_m K_L} + \frac{C_e}{Q_m} \tag{6}$$

where Q_e (mg/g) is the amount of RhB adsorbed at equilibrium per unit mass of adsorbent; C_e (mg/L) is the concentration of OFL at equilibrium; Q_m(mg/g) is the maximum RhB adsorption capacity; and k_L (L/mg) is the Langmuir constant, which is associated with the energy of adsorption.

The Freundlich model is expressed as:

$$\ln Q_e = \ln K_F + \frac{1}{n}\ln C_e \tag{7}$$

where C_e (mg/L) is the adsorption concentration at equilibrium, Q_e (mg/g) is the equilibrium adsorption capacity, K_F is the Freundlich constant, and *1/n* is a constant associated with the adsorption intensity or surface heterogeneity. The values of K_F and *1/n* can be obtained from a plot of ln Q_e against ln C_e.

The Dubinin-Radushkevich model is given as:

$$\ln Q_e = \ln Q_m - \beta\varepsilon^2 \tag{8}$$

$$\varepsilon = RTln\left(1 + \frac{1}{C_e}\right) \tag{9}$$

$$E = \frac{1}{(2\beta)^{\frac{1}{2}}} \tag{10}$$

where Q_e (mg/g) is the amount adsorbed at the adsorption equilibrium, Q_m (mg/g) is the maximum adsorption capacity, β (kJ^2/mol^2) is a constant corresponding to the adsorption energy, ε is the Polanyi potential, R is the ideal gas constant [8.314 J/(mol K)], E (kJ/mol) is the average adsorption free energy, and T (K) is the thermodynamic temperature. The Q_m and β values were obtained from the intercept and slope, respectively, of the fitted line.

2.6. Adsorption thermodynamics

The thermodynamic behavior of RhB adsorption onto the AWBC was evaluated by measuring the change in free energy (ΔG), enthalpy (ΔH), and entropy (ΔS). The thermodynamic coefficients were determined according to adsorption experiments at temperatures ranging from 298 to 308 K using the following equations [21]:

$$\ln K_L = \frac{\Delta S}{R} - \frac{\Delta H}{RT} \tag{11}$$

$$\Delta G = -RT\ln K_L \tag{12}$$

where R is the ideal gas constant [8.314 J/(mol K)], K_L (L/mol) is the Langmuir isotherm constant, T (K) is the thermodynamic temperature of the solution, ΔG is the standard Gibbs free energy change, ΔH is the enthalpy change, and ΔS is the entropy change.

3. Results and discussion

3.1. BC characterization

From the SEM analysis, the surface morphology of AWBC before and after adsorption with RhB is shown in Figs. 1a–b. Before adsorption, the surface was coarse and heterogeneous, with a large number of pores with variable volumes (Fig. 1a). This pores are formed due to organic polymers such as cellulose, lignin and hemicellulose exists in the alligator weed. When the material was carbonized in high temperature, biological polymer became the tar and volatile matter, and the volatiles can produce hole [22]. Fig. 1b shows that a large number of holes on the AWBC surface are filled with RhB molecules after adsorption, indicating that AWBC can adsorb RhB into the pores formed from the pyrolysis.

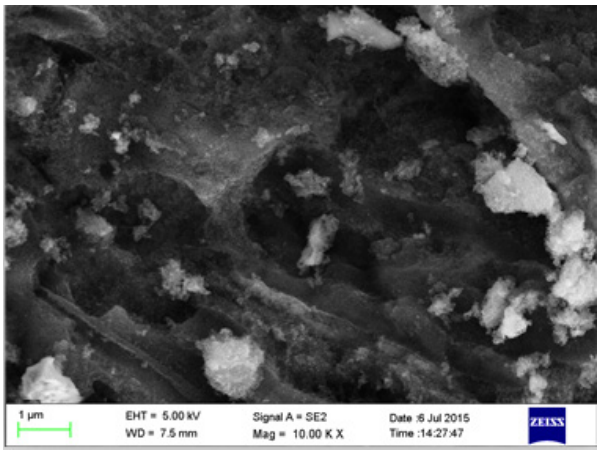

(a)

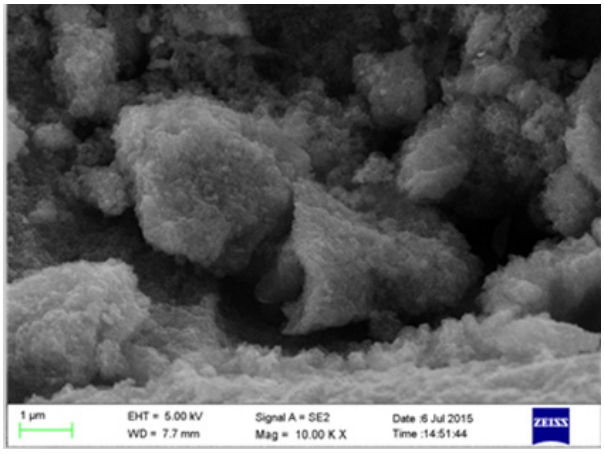

(b)

Fig. 1. The SEM of AWBC before (a) and after (b) RhB sorption.

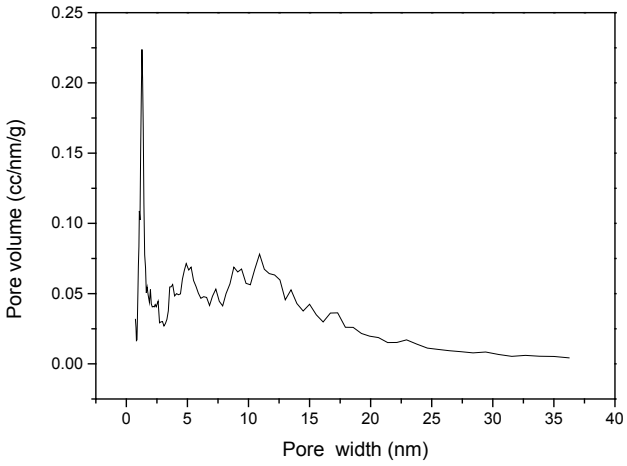

Fig. 2. AWBC pore size distributions.

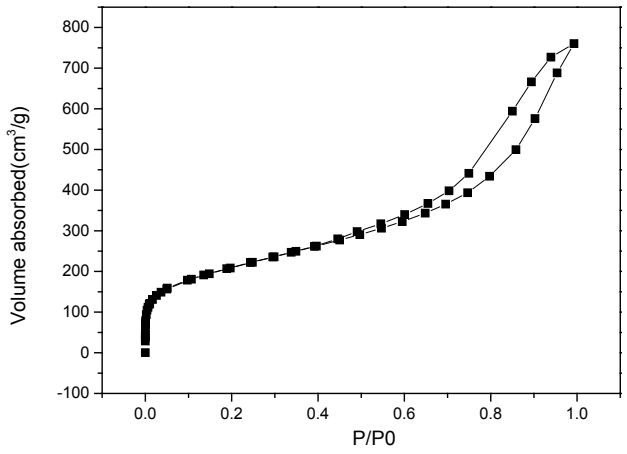

Fig. 3. AWBC N_2 adsorption/desorption isotherms.

The variability of the AWBC pore diameter is shown in Fig. 2. The pore diameter was mostly distributed as micropores of 0–2.0 nm and mesopores of 2.0–50 nm. No macropore structure was detected; therefore, the AWBC pore is considered to be a typical micropore/medium hole mixing structure. The hybrid structure of this micropore/medium hole can confer improved adsorption performance. Micropores and mesopores accounted for 17.6% and 82.4% of the total surface area, respectively, and the average pore size of the aperture structure was 4.05 nm. The micropore determines the total specific surface area of activated carbon [23]; However, a large number of mesopores play a channel role between the biochar molecules and RhB molecules, which can significantly improve the significantly improve the adsorption capacity of the AWBC particles for large and small molecules. This kind of aperture structure could significantly improve the adsorption capacity of the AWBC particles for large and small molecules. The N_2 adsorption/desorption isotherms are shown in Fig. 3. The AWBC adsorption isotherm is a type IV physisorption isotherm, indicating that the many mesopores are primarily involved in RhB adsorption [24]. The BET surface area of the AWBC was calculated to be 736.3 m^2/g, which is higher than that of an adsorbent prepared from bamboo (375.5 m^2/g), brazilian pepper (234.7 m^2/g), sugarcane bagasse (388.3 m^2/g), hickory wood (401.0 m^2/g) [25], mixed wood cuttings (273.6m^2/g), and rice husks (10.9 m^2/g) [26].

The comparison of the FTIR spectra examining the surface chemistry of AWBC before and after RhB adsorption is presented in Fig. 4. Before the RhB adsorption, the peak wavelength was in the 3417–3427 cm^{-1} range, which represents the telescopic vibration of the O-H functional group indicating the presence of tightly bound water molecules in AWBC. After RhB adsorption, this peak disappeared, presumably because free O-H functional groups bound to the hydrolytic RhB ion and thereby the detectable O-H content was reduced [27]. The peak 2921 cm^{-1} wavelength corresponds with the predicted vibration wavelength of the C-H group, and decreases slightly after RhB adsorption [28]. We identified a new peak in the 1300–1500 cm^{-1} wavelength range after RhB adsorption. This peak may be due to the O-H and CH_2 groups on the AWBC surface reacting with or being covered with hydrolyzed RhB ions. The peak at the 1176 cm^{-1} wavelength is associated with the telescopic vibration of C-O-C functional groups, while the peaks at 1645 cm^{-1} and 1632 cm^{-1} wavelengths before and after RhB

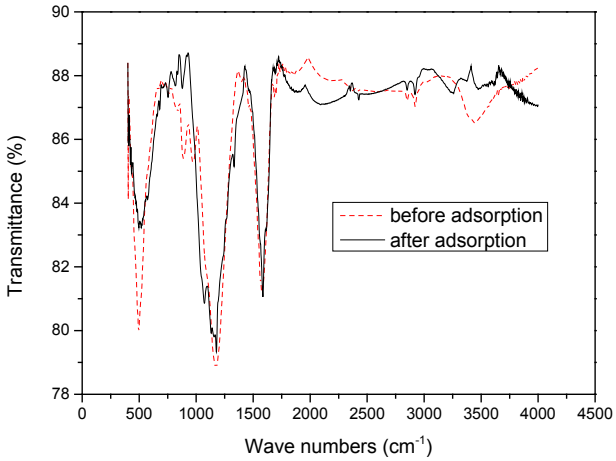

Fig. 4. FTIR spectra of the AWBC adsorbent before and after RhB adsorption.

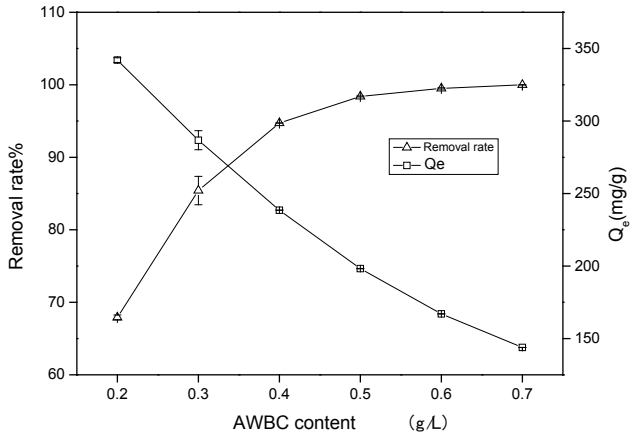

Fig. 5. Effect of AWBC dose on the RhB removal rate and adsorption capacity. The initial RhB concentration (100 mg/L), temperature (298 K), time (4 h) and pH are unadjusted.

adsorption on AWBC are associated with the telescopic vibration of C=C [29].

3.2. Adsorption studies

3.2.1. Effects of the adsorbent dosage

The effect of the AWBC adsorbent on the removal rate and the adsorption capacity at equilibrium adsorption is shown in Fig. 5. With increasing adsorbent dosage up to 0.4 g/L, the RhB removal rate increased rapidly to 95%; and thereafter, the removal rate increased gradually with increasing dosage. This pattern is attributable to there being many free sites on the AWBC adsorbent surface at the initial stages of adsorption, such that RhB hydrolysis molecules can rapidly occupy and combine with these sites [30]. With the increase of the dosage, the available sites on the surface of the adsorbent are gradually saturated, and the binding rate is decreased between the AWBC adsorbent and the RhB molecule [31]. Considering both the removal rate and the equilibrium adsorption capacity, when the removal rate was close to 100%, addition of more AWBC adsorbent to the RhB solution did not alter the removal rate, but reduced the adsorption capacity. Therefore, an adsorbent dosage of 0.4 g/L was selected for subsequent experiments to achieve optimal RhB removal and the most efficient use of the AWBC.

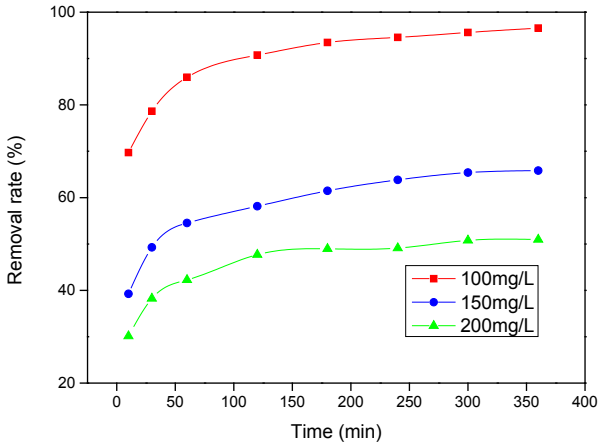

Fig. 6. Effect of contact time on the RhB removal rate by AWBC. The initial RhB concentration (100, 150, or 200 mg/L), adsorbent dosage (0.4 g/L), temperature (298 K) and pH are unadjusted.

3.2.2. Effects of contact time and RhB concentration

The effects of different contact times and RhB concentrations on the AWBC adsorption properties are shown in Figs. 6 and 7. The RhB removal rate decreased with increasing initial RhB concentrations (Fig. 6), whereas the adsorption capacity increased with increasing RhB concentrations (Fig. 7). The removal rate and adsorption capacity increased rapidly over the first 30 min, but then only gradually increased after 30 min. This is presumably due to there being a larger number of vacant active sites on the AWBC surface at the beginning of the adsorption process. The RhB hydrolytic molecules are likely to dif-

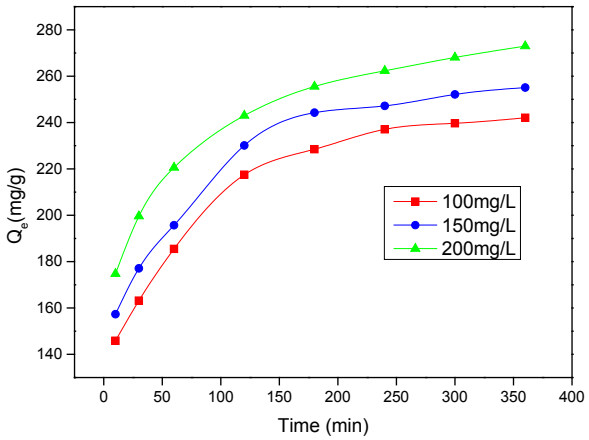

Fig. 7. Effect of contact time on the RhB removal rate by AWBC. The initial RhB concentration (100, 150, or 200 mg/L), adsorbent dosage (0.4 g/L), temperature (298 K) and pH are unadjusted.

fuse rapidly into the AWBC pore structures in the boundary layer, and then enter the internal pores. This explains the significantly higher removal rate and adsorption capacity in the first 30 min of adsorption. With prolonged adsorption time, the pore structure is likely to be increasingly occupied with RhB molecules, such that the number of vacant active sites decreases. This leads to a slowing down of the adsorption process and ultimately reaching a stable state [32]. Additionally, with an increase in the initial RhB solution concentration, the adsorption capacity also increased. This may be attributed to interactions between the AWBC surface functional groups and the RhB molecules [33]. The adsorption curves were smooth and continuous; indicating that adsorption of the RhB dye on the AWBC surface may represent the adsorption of single molecular layer. After the adsorption time reached 240 min, the removal rate and equilibrium adsorption capacity gradually plateaued. The adsorption at 240 min was therefore selected as the equilibrium time in subsequent experiments.

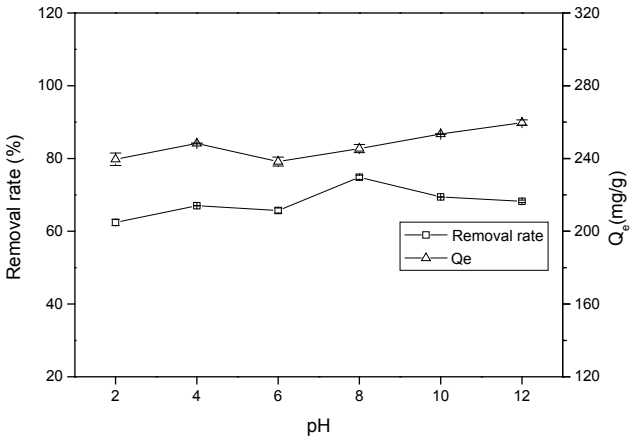

Fig. 8. Effect of solution pH on the RhB removal rate and AWBC adsorption capacity. The initial RhB concentration (100 mg/L), adsorbent dosage (0.4 g/L), time (4 h) and temperature (298 K) are unadjusted.

3.2.3. Effects of the solution pH

The influence of the solution pH on the removal rate and equilibrium adsorption capacity is shown in Fig. 8. At the pH ranges from acidic to alkaline, the removal rate is remains stable at approximately 70%, the equilibrium adsorption capacity is also stable at 250 mg/g, and RhB is mainly present in the form of cations in the aqueous solution. These result suggest that the degree of deprotonation of AWBC does not interfere with the hydrolysis of RhB molecules, and confirm previous findings that the effect of pH on adsorption performance is not significant [34]. In light of these results, the pH was not adjusted in subsequent experiments exploring single-factor effects.

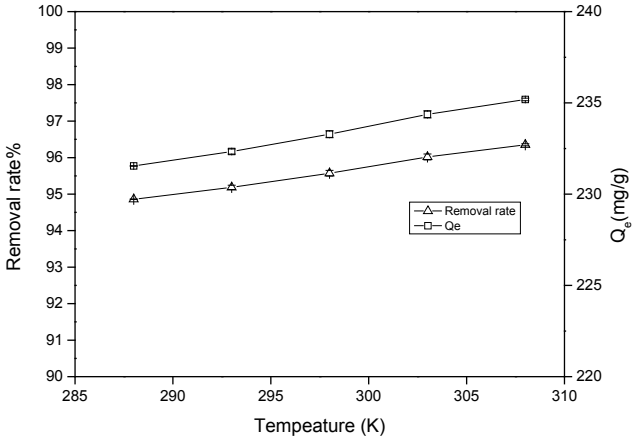

Fig. 9. Effect of temperature on the RhB removal rate and AWBC adsorption capacity. The initial RhB concentration (100 mg/L), adsorbent dosage (0.4 g/L), time (4 h) and pH are unadjusted.

3.2.4. Effects of temperature

The effect of temperature on the removal rate and equilibrium adsorption capacity of RhB is shown in Fig. 9. The removal rate and equilibrium adsorption capacity increased gradually with increasing temperature. This effect may be due to high temperatures promoting interactions between RhB and the AWBC surface functional groups. Previous work has shown that the attractant properties of adsorbent molecules on the AWBC surface are strengthened with elevated temperatures, indicating that the adsorption of RhB to AWBC is an endothermic process [35]. Nevertheless, the remainder of our experiments were carried out at RT (298 K), in order to explore the influences of other single factors on AWBC adsorption performance.

3.2.5. Kinetic models

Table 1 summarizes the parameters of the three kinetic models of RhB adsorption. Our results supported the pseudo-first-order and pseudo-second-order models, with high R^2 values ($R^2 > 0.997$); which shows that both models can describe the adsorption mechanism. Under the three different concentrations of 100, 150 and 200 mg/L, the R^2 values of the pseudo-second-order model were close to 1 (0.9998, 09999 and 0.9996, respectively). The adsorption of the pseudo-second-order model is therefore dominant, indicating that the adsorption rate is primarily controlled by the exchange or sharing of electrons to participate in the chemical adsorption of valence forces [36]. The diffusion model for the particles in the RhB adsorption is shown in Fig. 10. In this model, the adsorption process was divided into two stages. In the first stage, RhB adsorbed to the AWBC surface and the adsorption capacity increased rapidly. In the second stage, the adsorption was affected by the particle diffusion rate, and the adsorption process slowed down [37]. Initially, RhB dye molecules rapidly gather on the outer AWBC surface through the liquid membrane. They then enter the interior of the AWBC surface and adsorb to the inner surface, and then finally reach an equilibrium state of adsorption [38]. The adsorption of alkaline dye by alligator weed is therefore attributed to the combination of outer membrane diffusion and internal diffusion.

Table 1
Pseudo-first-order and pseudo-second-order kinetic parameters and particle diffusion kinetics for the adsorption of RhB by AWBC at different temperatures

Concentration C_e (mg/L)	Exp-data Q_e (mg/g)	Pseudo-first-order kinetics			Pseudo-second-order kinetics				Particle diffusion kinetic		
		k_1 (min^{-1})	Q_e ($mg{\cdot}g^{-1}$)	R^2	k_2 ($g{\cdot}mg^{-1}{\cdot}min^{-1}$)	Q_e ($mg{\cdot}g^{-1}$)	V_0 ($mg{\cdot}g^{-1}{\cdot}min^{-1}$)	R^2	k_p ($mg{\cdot}g^{-1}{\cdot}min^{-1/2}$)	C ($mg{\cdot}g^{-1}$)	R^2
100	237	0.0176	70	0.9939	0.00056	244	33.22	0.9998	3.9321	175.5	0.8852
150	256	0.0128	88	0.9760	0.00030	250	18.98	0.9999	4.9177	160.75	0.9809
200	264	0.0277	150	0.9840	0.00033	270	24.10	0.9996	6.2697	161.16	0.8663

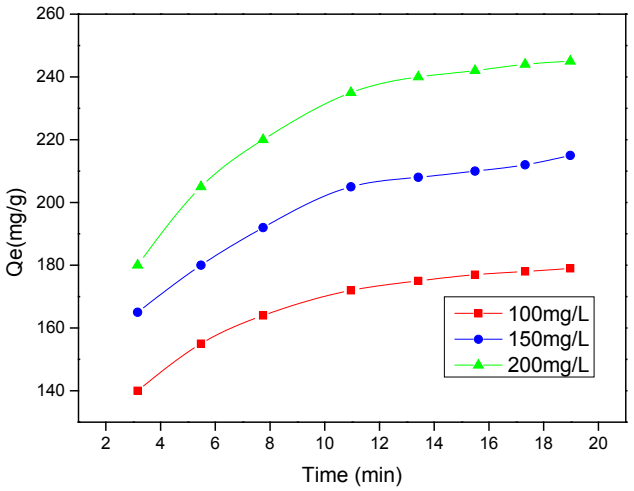

Fig. 10. Plot of the intraparticle diffusion model for adsorption of RhB onto AWBC. The initial RhB concentration (100, 150, or 200 mg/L), adsorbent dosage (0.4 g/L), temperature (298 K), and pH are unadjusted.

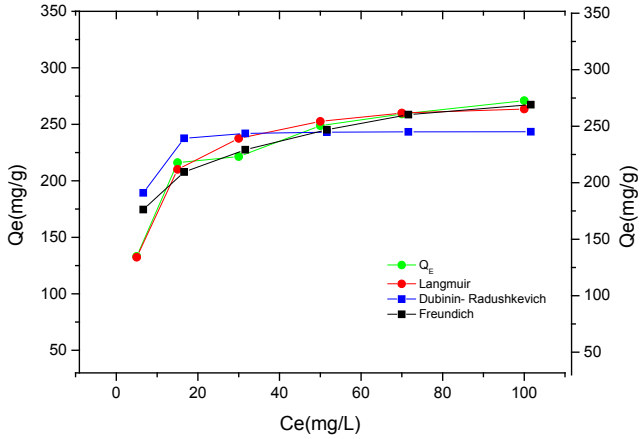

Fig. 11. Comparison of experimental data with models at 298 K.

3.3. Adsorption isotherms

The adsorption isotherms model experimental data parameters are shown in Table 2. The R^2 values for the Langmuir and Freundlich models were greater than 0.99 (0.9981, 0.9967, 0.9972) and 0.97 (0.9784, 0.9818, 0.9895), respectively; indicating that these models are the most appropriate for this adsorption. Additionally, the comparison between the date of Q_e and the Q_m in the three models is shown in Fig. 11. The data suggests that the Langmuir model best describes the adsorption mechanism at 288 K. This result supports previous work that showed that the adsorption of RhB by AWBC is a monolayer adsorption process, and the adsorption of RhB occurred on the adsorbents surface [39]. Additionally, while $K_L > 0$, $1/n$ values in the Freundlich model were between 0 and 1 at all three temperatures, indicating that adsorption is a favorable process [40]. Finally, the Dubinin-Radushkevich model did not describe the adsorption process very well in comparison with the other two models. The simulated Q_m was quite different from the Q_e in the experimental data, and had a relatively low correlation coefficient ($R^2 < 0.90$).

3.4. Adsorption thermodynamics

The adsorption thermodynamics of RhB to AWBC are shown in Table 3. Thermodynamic parameters depict the

Table 2
Langmuir, Freundlich, and Dubinin-Radushkevich model and correlation coefficients for adsorption of RhB by AWBC at different temperatures

Temperature/K	Langmuir model			Freundlich model			Dubinin-Radushkevich model			
	Q_m/(mg/g)	K_L/(L/mg)	R^2	$1/n$	K_F/$(mg/g)^{1/n}$	R^2	β (mol^2/J^2)	Q_m (mg/g)	E (kJ/mol)	R^2
288	250	0.2614	0.9981	0.1113	146.9217	0.9784	3.0×10^{-6}	244	408	0.4032
298	278	0.2034	0.9967	0.1410	142.7079	0.9818	1.0×10^{-6}	245	707	0.7576
308	286	0.3333	0.9972	0.1449	151.1995	0.9895	6.0×10^{-6}	272	289	0.8694

Table 3
The thermodynamic parameters of adsorption of RhB on AWBC at different temperatures

T(K)	K/(L/mol)	ΔG (kJ/mol)	ΔS (J/mol K)	ΔH (kJ/mol)
288	118837	–27.98	126	8.6
298	92451	–28.33		
308	151515	–30.55		

endothermic nature of adsorption process of RhB to AWBC is a spontaneous endothermic process. The negative Δ*G* value indicates the degree of favorability of the RhB adsorption and shows that it occurs spontaneously. The positive enthalpy change, ΔH, indicates that the adsorption process belongs to an endothermic reaction. This result is consistent with the increase in the maximum adsorption capacity simulated by the Langmuir isotherm model with increasing temperature [41]. Additionally, the positive entropy change, ΔS, indicates that the adsorption of RhB by AWBC increases the disorder of the molecules at the solid-liquid interface.

3.5. Orthogonal experiments

The results of orthogonal experiments examining four factors at three levels of AWBC adsorbed RhB are shown in Table 4 and Table 5. The results indicated that the combination of an AWBC dosage of 0.6 g/L, an initial RhB concentration of 100 mg/L, 288 K and pH 12 achieved the optimal adsorption efficiency based on the maximum removal rate. The importance of the each of the four factors on the adsorption efficiency obtained from range analysis were AWBC dosage > pH > initial concentration > temperature. It can be concluded that the AWBC dosage has the most significant effect on the adsorption capacity, while temperature has the least influence. This finding is consistent our single-factor experimental results.

Table 4
Orthogonal test design of AWBC adsorb RhB

Test number	pH	Temperature (K)	Concentration (mg/l)	AWBC dosage (g/l)	Removal rate (%)	Equilibrium adsorption (mg/g)
1	1	288	150	0.4	64.07	255.50
2	7	288	50	0.2	77.76	100.60
3	12	288	100	0.6	97.96	257.2
4	7	298	100	0.2	59.15	155.30
5	12	298	150	0.6	89.66	357.58
6	1	298	50	0.4	97.66	126.35
7	12	308	50	0.6	99.97	129.33
8	1	308	100	0.2	51.17	134.35
9	7	308	150	0.4	73.94	294.88

Table 5
The orthogonal experiment result and range analysis of adsorption of RhB on AWBC

	Level	pH	Temperature (K)	Concentration (mg/l)	AWBC dosage (g/L)
	K1	212.9	239.79	275.39	188.08
	K2	210.85	246.47	208.28	235.67
	K3	287.59	225.08	227.67	287.59
Adsorption efficiency	K1	70.97	79.93	91.80	62.69
	K2	70.28	82.16	69.43	78.56
	K3	95.86	75.03	75.89	95.86
	R	25.58	7.13	22.37	33.17
Adsorption capacity	K1	516.2	613.3	356.28	390.25
	K2	550.78	639.23	546.85	676.73
	K3	744.11	558.56	907.96	744.11
	K1	172.07	204.43	118.76	130.08
	K2	183.59	213.08	182.28	225.58
	K3	248.04	186.19	302.65	248.04
	R	75.97	26.89	183.89	117.96

4. Conclusions

In this work, alligator weed was used as an activator for preparation of biochar. SEM showed that the adsorption created a coarse and heterogeneous surface with a large number of pores with variable volumes. The AWBC surface area was 736.3 m^2/g, and the average pore size was 4.05 nm. FTIR analysis showed that phosphorus-containing functional groups, as well as C–H, C–O, and C=C species, were present on the AWBC surface; which may enhance the RhB adsorption efficiency. The RhB adsorption kinetics correlated well with a pseudo-second-order kinetic model (R^2> 0.997), and this is considered to 7 be the rate-limiting factor. The batch equilibrium data fitted well to the Langmuir isotherm model; indicating monolayer adsorption and an adsorption capacity of 286 mg/g (R^2 = 0.9972). Negative ΔG values confirmed the spontaneity of the adsorption process, while positive ΔH and ΔS values indicated endothermic and irreversible adsorption. The orthogonal experiments showed that of the four factors affecting adsorption efficiency obtained from our range analysis, AWBC dosage > pH > initial concentration >temperature. Therefore, AWBC dosage has a significant effect on the adsorption capacity, while temperature has the least effect. AWBC is likely to be an effective and low-cost material for removing RhB from aqueous wastewater.

Acknowledgments

This work was supported by the National Major Science and Technology Program for Water Pollution Control and Treatment (2017ZX07101-001), National Natural Science Foundation of China (No. 51708340 and No.51608315), Promotional Research Fund for Excellent Young and Middle-aged Scientists of Shandong Province (ZR2016CB18) and a Project of Shandong Province Higher Educational Science and Technology Program (No. J15LE07).

References

[1] O.J. Hao, H. Kim, P.C. Chiang, Decolorization of Wastewater, C R C Crit. Rev. Environ. Contr., 30 (2000) 449–505.
[2] S.C. Santos, V.J. Vílar, R.A. Boaventura, Waste metal hydroxide sludge as adsorbent for a reactive dye, J. Hazard. Mater., 153 (2008) 999–1008.
[3] V.V.B. Rao, S.R.M. Rao, Adsorption studies on treatment of textile dyeing industrial effluent by flyash, Chem. Eng. J., 116 (2006) 77–84.
[4] V.K. Gupta, Suhas, I. Ali, V.K. Saini, Removal of Rhodamine B, Fast Green, and Methylene Blue from wastewater using red mud, an aluminum industry waste, Ind. Eng. Chem., 43 (2004) 1740–1747.
[5] S.K. Das, P. Ghosh, I. Ghosh, A.K. Guha, Adsorption of rhodamine B on Rhizopus oryzae: Role of functional groups and cell wall components, Colloid. Surface. B., 65 (2008) 30–34.
[6] A.K. An, J. Guo, S. Jeong, E.J. Lee, S.A. Tabatabai, T. Leiknes, High flux and antifouling properties of negatively charged membrane for dyeing wastewater treatment by membrane distillation, Water Res., 103 (2016) 362–371.
[7] Q. Sun, L. Yang, The adsorption of basic dyes from aqueous solution on modified peat-resin particle, Water Res., 37 (2003) 1535–1544.
[8] A.K. Verma, P. Bhunia, R.R. Dash, Effectiveness of aluminum chlorohydrate (ACH) for decolorization of silk dyebath effluents, Ind. Eng. Chem., 51 (2013) 8646–8651.
[9] L.p.-G. V, G.r. MC, Decolourisation of simulated reactive dyebath effluents by electrochemical oxidation assisted by UV light, Chemosphere, 62 (2006) 106–112.
[10] H. Zou, W. Ma, Y. Wang, A novel process of dye wastewater treatment by linking advanced chemical oxidation with biological oxidation, Arch. Environ Prot., 41 (2015) 33–39.
[11] W. Ou, G. Zhang, X. Yuan, P. Su, Experimental study on coupling photocatalytic oxidation process and membrane separation for the reuse of dye wastewater, J. Water Pro. Eng., 6 (2015) 120–128.
[12] Q. Wang, Z.K. Luan, N. Wei, J. Li, C.X. Liu, The color removal of dye wastewater by magnesium chloride/red mud (MRM) from aqueous solution, J. Hazard. Mater., 170 (2009) 690.
[13] Y. Guo, D.A. Rockstraw, Activated carbons prepared from rice hull by one-step phosphoric acid activation, Micropor. Mesopor. Mat., 100 (2007) 12–19.
[14] S.S. Tahir, N. Rauf, Removal of a cationic dye from aqueous solutions by adsorption onto bentonite clay, Chemosphere, 63 (2006) 1842–1848.
[15] I.D. Mall, V.C. Srivastava, N.K. Agarwal, Removal of Orange-G and Methyl Violet dyes by adsorption onto bagasse fly ash—kinetic study and equilibrium isotherm analyses, Dyes Pigments, 69 (2006) 210–223.
[16] M.A. Alghouti, M.A. Khraisheh, S.J. Allen, M.N. Ahmad, The removal of dyes from textile wastewater: a study of the physical characteristics and adsorption mechanisms of diatomaceous earth, J. Environ. Manage., 69 (2003) 229–238.
[17] D. Clements, T.M. Dugdale, K.L. Butler, T.D. Hunt, Management of aquatic alligator weed (Alternanthera philoxeroides) in an early stage of invasion, Manage. Bio. Inva., 5 (2014) 327–339.
[18] H.M. Xu, G.F. He, M.T. Shi, J. Tu, W. Liu, W.N. Xiang, Preparation and characterization of mesoporous activated carbon from alligator weed with H_3PO_4, Adv. Mater. Res., 936 (2014) 868–874.
[19] G. Yang, H. Chen, H. Qin, Y. Feng, Amination of activated carbon for enhancing phenol adsorption: Effect of nitrogen-containing functional groups, Appl. Surf. Sci., 293 (2014) 299–305.
[20] M. Ghaedi, S.N. Kokhdan, Oxidized multiwalled carbon nanotubes for the removal of methyl red (MR): kinetics and equilibrium study, Desal. Water Treat., 49 (2012) 317–325.
[21] M. Ghaedi, B. Sadeghian, A.A. Pebdani, R. Sahraei, A. Daneshfar, C. Duran, Kinetics, thermodynamics and equilibrium evaluation of direct yellow 12 removal by adsorption onto silver nanoparticles loaded activated carbon, Chem. Eng. J., 187 (2012) 133–141.
[22] O. Das, A.K. Sarmah, The love-hate relationship of pyrolysis biochar and water: A perspective, Sci. Total Environ., 512–513 (2015) 682–685.
[23] K.L. Foster, The role of micropore size and chemical nature of the pore surface on the adsorption properties of activated carbon fibers,Nuclear Magnetic Shieldings and Molecular Structure. Springer Netherlands. 1993, pp. 160–165.
[24] K.S.W. Sing, Reporting physisorption data for gas/solid systems with special reference to the determination of surface area and porosity (Provisional), Pure Appl. Chem., 57 (2009) 603–619.
[25] Y. Yao, B. Gao, H. Chen, L. Jiang, M. Inyang, A.R. Zimmerman, X. Cao, L. Yang, Y. Xue, H. Li, Adsorption of sulfamethoxazole on biochar and its impact on reclaimed water irrigation, J. Hazard. Mater., 4 (2012) 408–413.
[26] S. Kizito, S. Wu, K.W. Kipkemoi, M. Lei, Q. Lu, H. Bah, R. Dong, Evaluation of slow pyrolyzed wood and rice husks biochar for adsorption of ammonium nitrogen from piggery manure anaerobic digestate slurry, Sci. Total Environ., 505 (2015) 102–112.
[27] M. Vithanage, A.U. Rajapaksha, M. Ahmad, M. Uchimiya, X. Dou, D.S. Alessi, S.O. Yong, Mechanisms of antimony adsorption onto soybean stover-derived biochar in aqueous solutions, J. Environ. Manage., 151 (2015) 443–449.
[28] J. Anandkumar, B. Mandal, Adsorption of chromium(VI) and Rhodamine B by surface modified tannery waste: Kinetic, mechanistic and thermodynamic studies, J. Hazard. Mater., 186 (2011) 1088.
[29] V.O.A. Tanobe, T.H.D. Sydenstricker, M. Munaro, S.C. Amico, A comprehensive characterization of chemically treated Brazilian sponge-gourds (Luffa cylindrica), Polym. Test., 24 (2005) 474–482.

[30] Q. Kong, Q. Liu, M.S. Miao, Y.Z. Liu, Q.F. Chen, C.S. Zhao, Kinetic and equilibrium studies of the biosorption of sunset yellow dye by alligator weed activated carbon, Desal. Water Treat., 66 (2017) 281–290.
[31] D. Kołodyńska, R. Wnętrzak, J.J. Leahy, M.H.B. Hayes, W. Kwapiński, Z. Hubicki, Kinetic and adsorptive characterization of biochar in metal ions removal, Chem. Eng. J.. 197 (2012) 295–305.
[32] Z. Qi, Q. Liu, Z.R. Zhu, Q. Kong, Q.F. Chen, C.S. Zhao, Y.Z. Liu, M.S. Miao, C. Wang, Rhodamine B removal from aqueous solutions using loofah sponge and activated carbon prepared from loofah sponge, Desal. Water Treat., 57 (2016) 1–13.
[33] N. Karakoyun, S. Kubilay, N. Aktas, O. Turhan, M. Kasimoglu, S. Yilmaz, N. Sahiner, Hydrogel–Biochar composites for effective organic contaminant removal from aqueous media, Desalination, 280 (2011) 319–325.
[34] F. Güzel, H. Sayğılı, G.A. Sayğılı, F. Koyuncu, Decolorisation of aqueous crystal violet solution by a new nanoporous carbon: Equilibrium and kinetic approach, J. Ind. Eng. Chem., 20 (2014) 3375–3386.
[35] Z.G. Liu, F.S. Zhang, Removal of lead from water using biochars prepared from hydrothermal liquefaction of biomass, J. Hazard. Mater., 167 (2009) 933–939.
[36] E.L. Cochrane, S. Lu, S.W. Gibb, I. Villaescusa, A comparison of low-cost biosorbents and commercial sorbents for the removal of copper from aqueous media, J. Hazard. Mater., 137 (2006) 198–206.
[37] Y. Wang, Q. Liu, L. Shu, M. Miao, Y. Liu, Q. Kong, Removal of Cr(VI) from aqueous solution using Fe-modified activated carbon prepared from luffa sponge: kinetic, thermodynamic, and isotherm studies, Desal. Water Treat., 57 (2016) 1–12.
[38] H. Lu, W. Zhang, Y. Yang, X. Huang, S. Wang, R. Qiu, Relative distribution of Pb^{2+} sorption mechanisms by sludge-derived biochar, Water Res., 46 (2012) 854.
[39] P. Wang, L. Tang, X. Wei, G. Zeng, Y. Zhou, Y. Deng, J. Wang, Z. Xie, W. Fang, Synthesis and application of iron and zinc doped biochar for removal of p-nitrophenol in wastewater and assessment of the influence of co-existed Pb(II), Appl. Surf. Sci., 392 (2017) 391–401.
[40] L. Tang, J. Yu, Y. Pang, G. Zeng, Y. Deng, J. Wang, X. Ren, S. Ye, B. Peng, H. Feng, Sustainable efficient adsorbent: Alkali-acid modified magnetic biochar derived from sewage sludge for aqueous organic contaminant removal, Chem. Eng. J., 336 (2018) 160–169.
[41] Z. Belala, M. Jeguirim, M. Belhachemi, F. Addoun, G. Trouvé, Biosorption of basic dye from aqueous solutions by Date Stones and Palm-Trees Waste: Kinetic, equilibrium and thermodynamic studies, Desalination, 271 (2011) 80–87.